J. Mech. Phys. Solids 212 (2026) 106576

Contents lists available at ScienceDirect

Journal of the Mechanics and Physics of Solids

journal homepage: www.elsevier.com/locate/jmps

Initiation of regularized cracks is explained by the coupled criterion

Aurélien Doitrand [a,*], Gergely Molnár [b]

[a] Univ Lyon INSA Lyon, Université Claude Bernard Lyon 1, CNRS UMR5510, MATEIS, F-69621, Villeurbanne, France
[b] CNRS, INSA Lyon, LaMCoS, UMR5259, 69621, Villeurbanne, France

ARTICLE INFO

Keywords:
Coupled criterion
Regularized crack
Matched asymptotic approach

ABSTRACT

Matched asymptotic expansions and phase-field regularization are combined to propose an implementation of the coupled criterion that accounts for the presence of an initial process zone. The initial process zone is introduced by prescribing phase-field Dirichlet boundary conditions around the crack initiation location, which allows us to study either sharp or regularized crack initiation through an initial process zone. An increase in the initially prescribed phase-field value enlarges the effective process zone and progressively reduces the stress singularity at the V-notch tip, showing that even a partially developed process zone can mitigate singular stresses through non-uniform stiffness, without requiring plastic regularization. Furthermore the process zone tends to decrease the incremental energy release rate, thus resulting in a higher initiation generalized stress intensity factor than the one obtained without an initial process zone. The findings reveal that, unlike Griffith's singular formulation, the phase-field model remains intrinsically regularized – even in the vanishing-length limit – raising the fundamental question of whether truly sharp cracks can exist or if a finite process zone always emerges through local structural rearrangement. The proposed approach thus extends the coupled criterion to study crack initiation and propagation in quasi-brittle materials.

1. Introduction

The fracture process zone (FPZ) refers to the region surrounding a crack tip where nonlinear and often irreversible deformation processes occur. This zone represents the transition from purely elastic behavior to the onset of inelastic mechanisms, making it a central concept in fracture mechanics. Early X-ray investigations by Irwin (1948) and Orowan (1949) revealed that even nominally brittle materials exhibit a finite zone of regularization near the crack front. Their findings led to the recognition that the actual critical energy release rate is several orders of magnitude greater than that predicted by Griffith's original model. Building on these insights, Barenblatt (1959) and Dugdale (1960) introduced theoretical models in which localized yielding near the crack tip produces cohesive tractions that cap the otherwise singular stress field.

Over the following decades, a variety of experimental approaches (Labuz et al., 1983; Chengyong et al., 1990; Denarie et al., 2001; Du et al., 1990; Guo et al., 1993; Yu and Kobayashi, 1994; Zang et al., 2000; Otsuka and Date, 2000; Zietlow and Labuz, 1998; Labuz et al., 1987) were developed to characterize the geometry and extent of the FPZ (Neimitz and Aifantis, 1987) in brittle and quasi-brittle materials. These studies generally interpret the FPZ as a damaged region around the crack tip, associated with irreversible microstructural rearrangements. Evidence of such zones has been reported in a wide range of materials, including concrete

* Corresponding author.
E-mail address: aurelien.doitrand@insa-lyon.fr (A. Doitrand).

https://doi.org/10.1016/j.jmps.2026.106576
Received 31 October 2025; Received in revised form 10 February 2026; Accepted 3 March 2026
Available online 6 March 2026
0022-5096/© 2026 Elsevier Ltd. All rights are reserved, including those for text and data mining, AI training, and similar technologies.

(Cedolin et al., 1983), granite (Labuz et al., 1983), geological faults (Vermilye and Scholz, 1998), wood (Yu et al., 2019), model composites (Haidar et al., 2005), and silica glass (Rountree et al., 2010). A comprehensive review of FPZ observations and interpretations is provided by Brooks (2013). Currently, digital image correlation (Réthoré and Estevez, 2013) is the most widely used method to quantify the FPZ, although alternative techniques remain effective for specific materials–such as optical methods in transparent polymers (Cortet et al., 2005) and X-ray imaging in concrete (Otsuka and Date, 2000).

However, whether a crack can exist in the absence of a process zone remains an open question, particularly concerning how crack initiation may transform a state without a process zone into one where such a zone develops, or conversely, how an existing process zone may vanish and a sharp crack can develop. Fracture mechanics models able to study crack nucleation generally rely on the idea of a coupling between energy and strength comparisons. These kinds of models include the material critical energy release rate (ERR) so as to retrieve Linear Elastic Fracture Mechanics (LEFM) when studying the propagation of sufficiently long cracks (Griffith, 1921, 1924; Irwin, 1958). In addition, the strength aspects may be incorporated in different ways. Cohesive zone models (Barenblatt, 1959; Dugdale, 1960) directly define the material strength surface through the tensile (σ_c) and shear (τ_c) strengths, as well as a criterion to define the strength under combined homogeneous tensile and shear loading (Benzeggagh and Kenane, 1996; Camanho and Dávila, 2002). For non-homogeneous loading conditions, *i.e.,* in the presence of a stress gradient, these critical strengths correspond to the onset of the damage mechanism through the creation of a process zone. Phase-field (PF) fracture models also define the material critical ERR as an input parameter, since they were initially thought and developed as a regularized Griffith's approach (Francfort and Marigo, 1998; Bourdin et al., 2000), through the definition of a characteristic length that provides a regularized description of a sharp crack. In these models, the material strength surface can also be defined, either as a direct input (Kumar et al., 2020; Doitrand et al., 2023b) or by defining the corresponding energy decomposition (De Lorenzis and Maurini, 2022; Vicentini et al., 2024). The magnitude of the strength surface can be indirectly set through the choice of the regularization length (Molnár et al., 2020, 2022).

The idea of coupling energy and strength criteria to study crack initiation was the cornerstone of the coupled criterion (CC) developed by Leguillon (2001, 2002). The combination of both criteria enables us to determine the initiation crack length and thus resolves the inability of LEFM to assess crack nucleation, still being consistent with it when studying the propagation of long enough cracks. The efficiency of the CC in understanding the details of crack initiation is highlighted in review papers (Weißgraeber et al., 2016; Doitrand et al., 2024). This is particularly marked when implementing the CC based on matched asymptotic expansions (Jiménez-Alfaro et al., 2025), which enables understanding the precise role of stress and energy contributions to crack nucleation (García and Leguillon, 2012; Felger et al., 2019; Doitrand et al., 2020; Jiménez-Alfaro and Leguillon, 2022).

Despite its great potential in understanding the underlying phenomenon of crack initiation, there are still a few pathological configurations for which the CC offers an incomplete failure description. Actually, the CC remains limited in some configurations for which the energy criterion predominates over the stress criterion. No characteristic length emerges from the coupling between strength and energy aspects, which is "disabled" since the CC thus reverts to a criterion solely based on energy (Molnár et al., 2025). In these configurations, the initiation load predicted by the CC becomes insensitive to the tensile strength. Two examples result in such a behavior:

i) Strong singularities (Leguillon et al., 2000; Leguillon and Murer, 2012; Aranda and Leguillon, 2023) are associated with asymptotic displacement fields varying as r^{λ}, (r is the distance to the singular point in polar coordinates), the characteristic exponent λ being smaller than 1/2. As a consequence, the IERR tends to infinity for vanishing crack lengths and the stress criterion is always satisfied, causing the CC to revert to an energy-only criterion.

ii) An asymptotic approach shows that the stress criterion has no influence on the initiation generalized stress intensity factor (GSIF) of a semi-infinite crack under remote anti-plane shear loading. The CC thus reverts to an energy-only criterion that predicts rectilinear propagation that maximizes the ERR (Mittelman and Yosibash, 2014, 2015; Doitrand et al., 2023a). However, experimental observations of the crack front rather show a series of facets inclined with respect to the initial crack propagation direction (Sommer, 1969; Knauss, 1970; Lazarus et al., 2008; Pham and Ravi-Chandar, 2014).

In the above-mentioned configurations where the CC fails to predict crack initiation due to the prevalence of the energy criterion, the missing ingredient to accurately describe the failure process could be the presence of a process zone prior to initiation. This ingredient, indeed considered in the phase-field approach that successfully describes the formation of facets under anti-plane shear (Molnár et al., 2024), appears as the main difference compared to the CC that generally considers the initiation of a sharp crack in an undamaged medium. So far, few works have addressed the possibility of incorporating a process zone in the CC. Leguillon and Yosibash (2017) implemented the matched asymptotic approach of the CC to study crack initiation at a V-notch tip with a small circular damage or plastic zone. The damage zone was described by a power-law decrease of the Young's modulus through a damage model based on singular elastic fields (Leguillon, 2008). The proposed approach enabled studying both the gradual damage zone growth and subsequent sudden crack initiation. Li et al. (2019) combined damage field determination based on continuum damage mechanics and discontinuous crack initiation based on the CC. They showed that damage zone growth and crack advance alternatively take place, leading to the formation of a damage band around the main sharp crack. In our previous work (Doitrand and Molnár, 2025), we extended the CC to study the initiation of a sharp crack surrounded by a process zone, employing the crack regularization offered in phase-field models. We showed that the proposed approach compared well with the phase-field model when calibrating the regularization length to the material strength surface. However, we did not consider the development of the process zone prior to crack initiation.

The objective of this work is thus to consider the presence of a process zone when assessing crack initiation with the CC. In Section 2, we first present how the process zone prior to crack initiation is described by using the regularization offered by

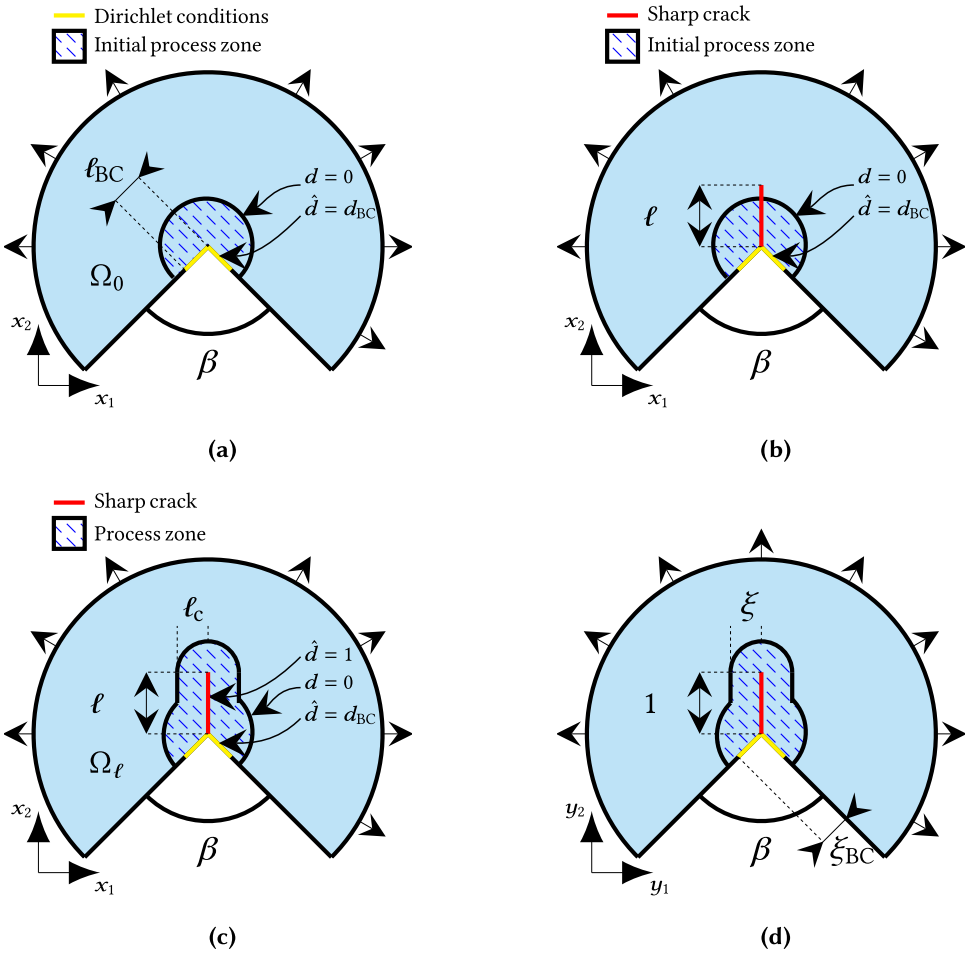

Fig. 1. (a) Representation of the configuration before crack initiation with a process zone (hatched zone described by the length ℓ_{BC} over which $\hat{d} = d_{BC}$ Dirichlet boundary conditions are applied, $0 < d_{BC} \leqslant 1$) at the V-notch tip (angle β). The damage variable d in the process zone varies between d_{BC} and 0 (pristine material). (b-c) Representation of the configurations after initiation of b) sharp (nominal length ℓ) or (c) regularized crack (regularization length ℓ_c) through the initial process zone. (d) Dimensionless problem corresponding to (c) when the coordinates are normalized by the sharp crack length (normalized length 1), involving the dimensionless regularization length $\xi = \ell_c/\ell$ and the dimensionless length $\xi_{BC} = \ell_{BC}/\ell$ over which Dirichlet boundary conditions are prescribed. The arrows correspond to the prescribed displacement at the boundary of the domain, far from the process zone and the initiation crack.

phase-field models and how it influences the stress fields before initiation. The formulation of the CC in the presence of an initial process zone is then presented in Section 3 before studying the case of a semi-infinite crack in an infinite medium in Section 4. We finally assess the influence of the initial process zone on sharp or regularized crack initiation at a V-notch (Section 5). The matched asymptotic expansions used to derive the CC formulation are described in the Appendix A.

2. Stress within the process zone

The overall methodology for investigating sharp and regularized crack initiation in the presence of a process zone is outlined in the following workflow: We first build the initial process zone, then compute the stress fields before initiation and the energy variation due to crack initiation, and finally solve the CC to determine the initiation length and GSIF. We study 2D crack initiation at a V-notch (angle β, *cf.* Fig. 1) under plane strain conditions and pure opening mode in a homogeneous isotropic quasi-brittle material (Young's modulus E, Poisson's ratio ν, critical ERR $\mathcal{G}_c$, Rankine's strength surface and tensile strength σ_c) in the presence of a process zone at the V-notch tip. The configuration just before crack initiation is depicted in Fig. 1(a). The process zone at the V-notch tip is described using the regularization offered by AT1 phase-field model (Pham et al., 2011), ℓ_c being the regularization length (implementation details are available in Molnár et al., 2022). The process zone is obtained by prescribing $\hat{d} = d_{BC}$ ($0 < d_{BC} \leqslant 1$) Dirichlet boundary conditions over a length ℓ_{BC} from the V-notch tip along the V-notch faces (Fig. 1(a)). In practice, Dirichlet boundary conditions are strongly enforced at each of the nodes located over a segment of length ℓ_{BC}. The process zone thus consists of a diffuse damage

zone around the V-notch tip, which is obtained by solving the phase-field equation without the elastic energy. The functional to minimize to determine the process zone shape thus reverts to the fracture energy $\int_{\Omega_0} \frac{G_c}{c_\omega \ell_c}\left(\omega(d)+\ell_c^2|\nabla d|^2\right)\mathrm{d}\Omega$, where $\omega(d)=d$ and $c_\omega = \int_0^1 \sqrt{\omega(s)}\mathrm{d}s = 8/3$, following AT1 PF model implementation (Molnár et al., 2022). The domain Ω_0 represents the uncracked entire body under investigation (see Fig. 1(a)). In the process zone, the damage variable d varies between d_{BC} (at the V-notch tip and faces) and 0 (out of the process zone). The parameters describing the process zone could be identified experimentally by local stiffness measurements, for instance using indentation, or through full-field measurements and primal and dual mode GSIF evaluation (Leguillon, 2011; Leguillon and Yosibash, 2017). The phase-field approximation replaces the discrete representation of the crack surface with an integral formulation based on a continuous damage variable (Bourdin et al., 2000). Consequently, in two dimensions, the in-plane effective process zone length, ℓ_{PZ}, is given by

$$\ell_{\mathrm{PZ}} = \frac{1}{c_\omega \ell_c}\int_{\Omega_0}\left(\omega(d)+\ell_c^2|\nabla d|^2\right)d\Omega. \tag{1}$$

Note that the process zone length tends towards ℓ_{BC} when ℓ_c tends towards 0.

Two problems are then studied from this initial configuration:

- **Sharp crack initiation at the V-notch tip**: This configuration is depicted in Fig. 1(b), where a sharp crack of length ℓ initiates through the process zone. In this configuration, we make the assumption that the initial process zone does not evolve during the sudden crack initiation. The crack may extend either inside or outside the process zone to cover all possible configurations that could be encountered experimentally.

- **Regularized crack initiation at the V-notch tip**: As depicted in Fig. 1(c), instead of a purely sharp description, the regularized crack is represented as a diffused damage zone around a sharp crack of nominal length ℓ. The corresponding domain Ω_ℓ is represented in Fig. 1(c). For the sake of simplicity, we use the same regularization length to describe the initial process zone and the regularized crack. The effective length of the regularized crack, ℓ_{eff}, is thus

$$\ell_{\mathrm{eff}} = \frac{1}{c_\omega \ell_c}\int_{\Omega_\ell}\left(\omega(d)+\ell_c^2|\nabla d|^2\right)d\Omega. \tag{2}$$

  As the regularization length approaches zero, the effective length ℓ_{eff} converges to the nominal crack length. The proposed model provides us with the option of implementing the coupled criterion using 3 input parameters (*i.e.,* tensile strength, critical ERR and regularization length). The definition of ℓ_c independently of the tensile strength permits the formulation of a third criterion. In this work, we rather choose to set the regularization length in order to retrieve a Rankine type strength surface, following the previously determined relation (Molnár et al., 2020, 2022; Doitrand and Molnár, 2025)

$$\ell_c = \eta\left(\nu, \frac{\sigma_{\mathrm{II}}}{\sigma_{\mathrm{I}}}\right)^2 \ell_{\mathrm{mat}}, \tag{3}$$

  where $\frac{\sigma_{\mathrm{II}}}{\sigma_{\mathrm{I}}}$ is the ratio of principal stresses and η is the normalized tensile strength and the Irwin's length is $\ell_{\mathrm{mat}} = \frac{EG_c}{\sigma_c^2}$.

Both problems are studied using the CC, presented in Section 3 and implemented through matched asymptotic expansions as detailed in the Appendix A. Finite element calculations are performed under small deformation assumptions in a dimensionless domain, *e.g.* represented in Fig. 1(d) which corresponds to the dimensional domain depicted in Fig. 1(c). This is called the "inner domain" in the matched asymptotic expansion formalism (see Appendix A for further details), in which the space variables are normalized by the sharp initiation crack length, which thus becomes 1. In the sequel, the variables ℓ_k indicate dimensional lengths whereas the variables ξ_k correspond to dimensionless lengths. In the inner domain, the initial process zone is described by:

- The normalized length over which phase-field Dirichlet conditions are prescribed along the V-notch faces, $\xi_{\mathrm{BC}} = \ell_{\mathrm{BC}}/\ell$.
- The magnitude of the damage variable along the V-notch faces, d_{BC}.
- The normalized regularization length, $\xi = \ell_c/\ell$.

Linear 4-node elements are used, the mesh is refined around the V-notch tip to ensure that the mesh size is not larger than 1/100 of the normalized sharp crack length and 1/10 of the dimensionless regularization length. This choice ensures that differences in the initiation loading smaller than 1% are obtained for finer meshes. The inner domain is artificially bounded at a normalized distance of $R = 400$, which is sufficiently large compared to ξ, ξ_{BC} and 1 (the normalized crack length) (Doitrand et al., 2020, 2023a). The boundary conditions prescribed at the inner domain artificial boundary (Fig. 1(d)) are the asymptotic displacement field corresponding to the opening mode at a V-notch. Three calculations are performed in the inner domain under identical displacement boundary conditions:

i) A calculation with the initial process zone present, but without a crack, performed in the inner domain corresponding to the configuration depicted in Fig. 1(a).
ii) A calculation with a sharp crack initiating through the initial process zone, performed in the inner domain corresponding to the configuration depicted in Fig. 1(b).
iii) A calculation with a regularized crack initiating through the initial process zone, performed in the inner domain (Fig. 1(d)) corresponding to the configuration depicted in Fig. 1(c).

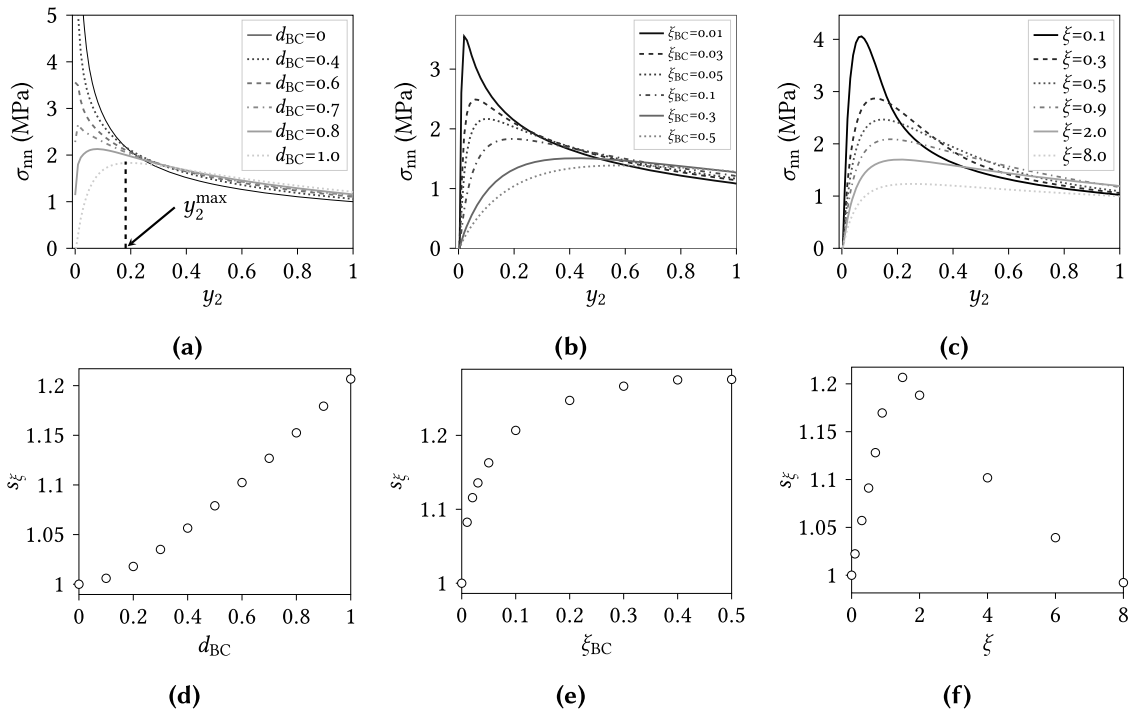

Fig. 2. (a-c) Opening stress variation as a function of the dimensionless distance to the V-notch tip (V-notch angle $\beta = 90$ deg.) along the V-notch bisector in the presence of a process zone and (d-f) opening stress value at the position of the sharp crack tip ($y_2 = 1$) before crack initiation obtained for a prescribed unit GSIF. (a) The coordinate at which the stress maximum is attained is noted $y_2^{\max}$. (a,d) Influence of the Dirichlet phase-field boundary condition magnitude d_{BC} for fixed $\xi_{BC} = 0.1$ and $\xi = 1.5$. (b,e) Influence of the length over which the boundary conditions are prescribed ξ_{BC}, for fixed $d_{BC} = 1$ and $\xi = 1.5$. (c,f) Influence of the regularization length ξ for fixed $\xi_{BC} = 0.1$ and $d_{BC} = 1$.

Among these models, only the geometry and the phase-field boundary conditions differ. The first calculation enables us to determine the stress field prior to crack initiation. Then, the second calculation allows us to study the initiation of a sharp crack (see Section 5.1) or of a regularized crack (see Sections 4 and 5.2) in the presence of an initial process zone. The dimensionless incremental energy release rate (IERR) A_{eff} (see Appendix A for further details) is obtained by calculating the elastic strain energy difference between the configuration containing only the process zone (without a crack) and the configuration featuring either a sharp or a regularized crack. Details on how the stress and the dimensionless IERR are computed through matched asymptotic expansions are given in the Appendix A.

Since the CC requires the knowledge of the stress field prior to crack initiation, it is essential to analyze how it is influenced by the initial process zone. At the leading order, the opening stress component is written as

$$\sigma_{nn} = K_I \ell^{\lambda-1} s_\xi, \tag{4}$$

where the parameter λ is the singularity exponent (see further details in the Appendix A) and s_ξ corresponds to the opening stress value at the sharp crack tip position before initiation. Is is obtained as the opening stress value for a unit imposed GSIF (K_I) before crack initiation in the inner domain.

The presence of the initial process zone has an influence on the stress fields along the notch bisector prior to crack initiation. Fig. 2 shows how the opening stress variation along the V-notch bisector is affected in the presence of the process zone for a $\beta = 90$ deg. V-notch angle. The first adjustable parameter to describe the initial process zone is d_{BC}. Fig. 2(a) shows the influence of d_{BC} on the stress variation along the V-notch bisector as a function of the normalized coordinate $y_2 = x_2/\ell$ (see Fig. 1(d)) for fixed $\xi_{BC} = 0.1$ dimensionless initial process zone length and $\xi = 1.5$ dimensionless regularization length. For d_{BC} values smaller than 0.6, the stress field remains singular and monotonically increases when approaching the V-notch tip. However, for d_{BC} values larger than 0.6, the damage field is sufficiently developed so that the singularity is mitigated and that the stress fields show a non-monotonic behavior near the V-notch tip. For instance, for d_{BC} larger than 0.8, the regularization makes the stress variation exhibiting a local maximum when approaching the V-notch tip. The location at which the stress is locally maximum is noted $y_2^{\max}$, it is 0 for sufficiently small d_{BC} or strictly positive for d_{BC} values larger than 0.7. In the particular case of $d_{BC} = 1$, we retrieve the stress field variation observed when employing classical phase-field approaches (Molnár et al., 2020; Abaza et al., 2022; Doitrand et al., 2023b). Fig. 2(d) shows the normalized opening stress value at the position of the sharp crack tip before initiation, which is further used to implement the CC (see Section 3), as a function of d_{BC}. This value is 1 in absence of process zone due to the normalization of the asymptotic stress field (Leguillon et al., 2007; Doitrand and Molnár, 2025) and shows an increasing trend with increasing d_{BC}. This variation can be

explained by the singularity mitigation due to the regularization. The larger d_{BC}, the smaller the stress near the V-notch tip, which increases the stress value further from the V-notch tip (*e.g.*, at the sharp crack tip position before initiation) to maintain the force balance for the same imposed loading.

This result is fundamental, since it demonstrates that in an elastic body, the introduction of a non-uniform stiffness field around the crack tip mitigates the singular stress. This result was previously obtained in the case of a Young's modulus vanishing at the V-notch tip and following a power law with a sufficiently small exponent (Leguillon, 2008; Leguillon and Yosibash, 2017; Ciavarella, 2024). Since the regularization tends to decrease the stiffness locally, it is noted that the strain fields remain singular even for the non-singular stress fields obtained with $d_{\mathrm{BC}} = 1$ at the V-notch tip. It is also shown here that a mitigation of the singular stress field can be obtained even in the case of a non vanishing Young's modulus at the V-notch tip (*e.g.,* for $0.6 < d_{\mathrm{BC}} < 1$). These findings are significant because they show that even in the absence of a plastic regularization, the singular stress field can be mitigated through a stiffness gradient, offering a potential alternative approach to strengthening materials with geometric singularities against cracking.

The second parameter describing the initial process zone is its dimensionless length from the V-notch tip along the V-notch faces, ξ_{BC}. Fig. 2(b) shows the influence of ξ_{BC} on the stress variation along the V-notch bisector as a function of the normalized coordinate for $d_{\mathrm{BC}} = 1$ and $\xi = 1.5$. Regardless of the length of the initial process zone, the stress field is no longer singular as it tends towards 0 when approaching the V-notch tip, exhibiting a maximum at $y_2 = y_2^{\max}$. As ξ_{BC} increases, the stress value at the peak decreases, while the normalized stress at the sharp crack tip increases (see Fig. 2(e)).

The third adjustable parameter to control the initial process zone is the dimensionless regularization length ξ, whose influence on the opening stress variation is shown in Fig. 2(c) for fixed $d_{\mathrm{BC}} = 1$ and $\xi_{\mathrm{BC}} = 0.1$. A non-singular stress field is obtained since $d_{\mathrm{BC}} = 1$, which tends towards zero when approaching the V-notch tip and shows a maximum. The larger the regularization length, the smaller the stress value at the maximum. However, the stress value at the sharp crack tip location before initiation shows a non-monotonic variation as a function of the normalized regularization length (Fig. 2(f)), increasing for ξ smaller than 2 then decreasing for larger values of the dimensionless regularization length. The description of the process zone thus has an influence on the stress field before initiation, which may influence the critical GSIF at initiation that can be determined using the CC, as explained in the next Section.

3. The coupled criterion

The CC enables us to study the initiation of a crack provided the simultaneous fulfillment of both stress and energy conditions (Leguillon, 2002):

- The opening stress must be larger than the material tensile strength σ_{c} along the crack path before initiation. In order to deal with the possibly non-monotonic stress variation due to the presence of the initial process zone (see Section 2), we have adapted the original formulation of the stress criterion (Leguillon, 2002; Leguillon et al., 2007) so that the tensile stress exceeds the material tensile strength at distances larger than the location of the peak stress, *i.e.,* : $\sigma_{\mathrm{nn}}(y_2) \geq \sigma_{\mathrm{c}} \ \forall \ y_2^{\max} \leqslant y_2 \leqslant 1$. The proposed stress criterion thus remains a nonlocal condition that has to be fulfilled all over the path between $y_2^{\max}$ and 1.
- The incremental energy release rate (IERR) must be larger than or equal to the critical ERR: $\mathcal{G}_{\mathrm{inc}}(\ell) \geq \mathcal{G}_{\mathrm{c}}$.

The IERR for a regularized crack in the presence of an initial process zone is defined as (See the Appendix A for further details)

$$\mathcal{G}_{\mathrm{inc}} = \frac{K_{\mathrm{I}}^2}{E} \ell^{2\lambda-1} A_{\mathrm{eff}}(d_{\mathrm{BC}}, \xi_{\mathrm{BC}}, \xi). \tag{5}$$

The dimensionless IERR is defined as $A_{\mathrm{eff}} = A(d_{\mathrm{BC}}, \xi_{\mathrm{BC}}, \xi)/\delta\xi_{\mathrm{eff}}$, where $A(d_{\mathrm{BC}}, \xi_{\mathrm{BC}}, \xi)$ is a scaling function computed in the inner domain and $\xi_{\mathrm{eff}} = \ell_{\mathrm{eff}}/\ell$ is the dimensionless effective crack length. The dimensionless IERR is obtained by computing, in the inner domain, the variation of elastic strain energy between i) the uncracked case in the presence of the initial process zone and ii) the configuration in the presence of either a sharp or a regularized crack.

The stress field prior to crack initiation can be computed using Eq. (4) (see the Appendix A and Section 2). The application of the CC reverts to combining the stress and the energy conditions previously described, which yields

$$\begin{cases} \frac{K_{\mathrm{I}}^2}{E} \ell^{2\lambda-1} A_{\mathrm{eff}}(d_{\mathrm{BC}}, \xi_{\mathrm{BC}}, \xi) \geq \mathcal{G}_c, \\ K_{\mathrm{I}} \ell^{\lambda-1} s_\xi(d_{\mathrm{BC}}, \xi_{\mathrm{BC}}, \xi) \geq \sigma_{\mathrm{c}}. \end{cases} \tag{6}$$

For a given combination of d_{BC} and ξ_{BC}, the two unknowns to determine are the initiation crack length ℓ_{i} and GSIF K_{Iapp} which are solutions of the equation system. For simplicity, in the following we will omit the dependence of A_{eff} and s_ξ on d_{BC} and ξ_{BC}. However, it should be kept in mind that the parameters of the initial process zone and the overall regularization length have a significant effect on the results. In the following equations, we thus provide the solution for the initiation crack length and related GSIF for fixed d_{BC} and ξ_{BC}.

The equation system Eq. (6) can be solved first for the initiation length

$$\ell = \frac{E\mathcal{G}_{\mathrm{c}} s_\xi^2(\xi_{\mathrm{c}})}{A_{\mathrm{eff}}(\xi_{\mathrm{c}})\sigma_c^2} = \ell_{\mathrm{i}}. \tag{7}$$

In this equation, the Irwin's characteristic length appears as $\ell_{\mathrm{mat}} = E\mathcal{G}_{\mathrm{c}}/\sigma_{\mathrm{c}}^2$. The dimensionless regularization length at initiation ξ_{c} is defined as $\xi_{\mathrm{c}} = \ell_{\mathrm{c}}/\ell_{\mathrm{i}}$. Accordingly, the initiation length can be expressed as a function of both the regularization length and

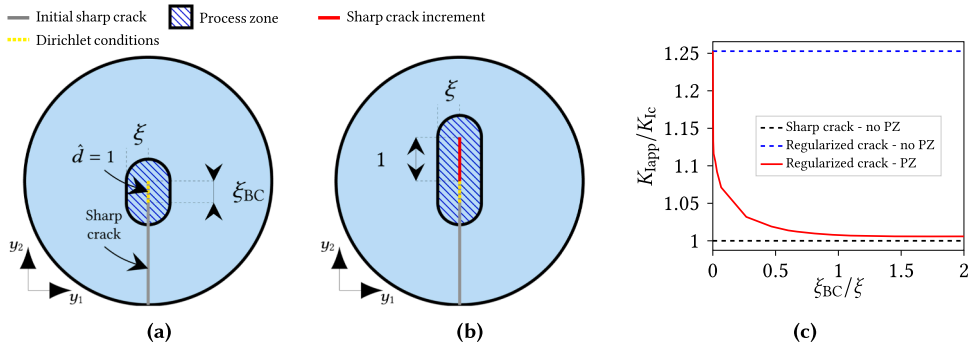

Fig. 3. Representation of the inner domain a) before and b) after crack propagation in the presence of an initial process zone. c) Variation of the normalized apparent stress intensity factor (SIF) at crack propagation as a function of the normalized initial process zone length (plain line) obtained for $\xi = 1.5$, the normalized apparent SIF values for a sharp and regularized crack without an initial process zone are also given as references (dashed lines).

Irwin's length as

$$\ell_{\mathrm{i}} = \frac{\ell_{\mathrm{c}}}{\xi_{\mathrm{c}}} = \ell_{\mathrm{mat}} \frac{s_{\xi}^2(\xi_{\mathrm{c}})}{A_{\mathrm{eff}}(\xi_{\mathrm{c}})}. \tag{8}$$

We recall that, in this general form, when ℓ_{c} is independent of the stress state, it gives the opportunity to introduce a third criterion within the CC framework. However, in this work, the regularization length is constrained in order to recover a Rankine-type strength surface, so that $\ell_{\mathrm{c}} = \eta^2 \ell_{\mathrm{mat}}$ (see Section 2). Consequently, the dimensionless regularization length and the critical initiation crack length can be determined by solving the following equation iteratively

$$\frac{A_{\mathrm{eff}}(\xi_{\mathrm{c}})}{\xi_{\mathrm{c}} s_{\xi}^2(\xi_{\mathrm{c}})} = \frac{1}{\eta^2}. \tag{9}$$

The initiation crack length can therefore be obtained either by evaluating the left member of Eq. (9) over a discrete crack length basis, or using Newton's method. For the latter, the convergence criterion is defined as a maximum relative error between two consecutive iterates of 10^{-8}. The initial guess can be chosen as a function of the Irwin's length ℓ_{mat}. Indeed, the initiation length is usually a fraction of ℓ_{mat}, either for sharp (Doitrand et al., 2020) or regularized (Doitrand and Molnár, 2025) cracks. For instance, the initial guess can be taken as $\ell_{\mathrm{mat}}/10$. The solution of Eq. (9) gives the dimensionless regularization length at initiation ξ_{c}, which also provides the initiation crack length ℓ_{i}. The apparent GSIF at initiation is finally obtained as

$$K_{\mathrm{Iapp}} = \left(\frac{E\mathcal{G}_{\mathrm{c}}}{A_{\mathrm{eff}}(\xi_{\mathrm{c}})}\right)^{1-\lambda} \left(\frac{\sigma_{\mathrm{c}}}{s_{\xi}(\xi_{\mathrm{c}})}\right)^{2\lambda-1}. \tag{10}$$

The initiation crack length and GSIF are thus obtained for fixed values of d_{BC} and ξ_{BC} by solving Eqs. (9) and (10).

4. Semi-infinite crack in infinite medium

We first illustrate the application of the proposed approach to study the propagation of a semi-infinite regularized crack in an infinite medium subjected to a remote tensile stress, see Fig. 3. The initial configuration, depicted in Fig. 3(a), consists of a semi-infinite sharp crack on which $\hat{d} = 1$ Dirichlet phase-field boundary conditions are prescribed over a dimensionless length ξ_{BC}. The configuration after the propagation of a regularized crack increment is shown in Fig. 3(b). In the case of an initial sharp crack, the singularity exponent is $1/2$, thus the term coming from the stress criterion in Eq. (10) is equal to 1. Therefore, the apparent stress intensity factor (SIF) at crack propagation, deduced from Eq. (10), writes

$$K_{\mathrm{Iapp}} = \sqrt{\frac{E\mathcal{G}_{\mathrm{c}}}{A_{\mathrm{eff}}(\xi_{\mathrm{c}})}}. \tag{11}$$

In the case of a purely sharp crack (*i.e.*, $\xi_{\mathrm{c}} = 0$), the relation between the critical SIF and critical ERR is found so that the crack propagates at $\mathcal{G} = \mathcal{G}_{\mathrm{c}}$ (or equivalently, $K_{\mathrm{Iapp}} = K_{\mathrm{I}} = K_{\mathrm{Ic}}$). It means that the proposed approach retrieves LEFM when studying the propagation of a semi-infinite sharp crack in infinite medium.

Otherwise, considering regularized crack propagation in the presence of the initial process zone, even if the stress-related term does not explicitly appear in the apparent SIF, the apparent SIF now depends on the material strength. Indeed, a change in the material strength induces a change in the regularization length (through Eq. (3)) and thus on the initial process zone description, which in turn influences the coefficient $A_{\mathrm{eff}}(\xi_{\mathrm{c}})$ and thus K_{Iapp}. The variation of the apparent SIF at crack propagation (normalized by the material critical SIF K_{Ic}) as a function of the ratio between the initial process zone length and the regularization length is shown in Fig. 3(c). As a matter of example, $\xi_{\mathrm{c}} = 1.5$ is chosen (in the order of magnitude of the value previously obtained for regularized crack initiation

without initial process zone Doitrand and Molnár, 2025; Abaza et al., 2022). Similar qualitative trends are obtained for other values of the normalized regularization length. The only difference obtained for other values of ξ_c is the value of K_{Iapp}/K_{Ic} when ξ_{BC} tends towards 0 (dashed blue line in Fig. 3(c)), which increases (resp. decreases) when ξ_{BC} increases (resp. decreases).

In the absence of an initial process zone, the studied configuration reverts to the nucleation of a regularized crack ahead of an initial sharp crack. The required apparent SIF to nucleate the regularized crack is around 25% larger than the material critical SIF. This is due to the fact that a part of the elastic strain energy is dissipated into the process zone creation, resulting in a higher required apparent SIF to make the initial sharp crack propagate as a regularized crack. This phenomenon was previously observed when implementing phase-field models of crack propagation from an initial sharp crack. Klinsmann et al. (2015) noticed overestimation in the ERR up to 25% for crack propagation under pure bending or in single edge notched specimens. Overall, they observed that crack initiation for a mesh induced initial crack always occurs with a significant delay compared to implementing the initial phase-field crack description. They thus challenged the claimed capability of the fracture phase-field method to find and accurately describe sharp crack initiation at arbitrary locations in a specimen. The overestimation of the nucleation load due to the choice of undamaged notch boundary conditions on the damage fields was also observed later by Singh et al. (2016), Sargado et al. (2018), Tanné et al. (2018), Kristensen et al. (2021). When increasing the initial process zone length, *i.e.,* the length over which the Dirichlet boundary conditions are prescribed over the initial crack, the apparent SIF at crack propagation decreases until it reaches a plateau that corresponds to the material critical stress intensity factor. It means that if the initial Dirichlet phase-field boundary conditions are prescribed over a sufficiently large zone, regularized crack propagation reverts to LEFM. Actually, prescribing the phase-field boundary conditions over a length at least equal to the regularization length yields a difference smaller than 1% on the SIF at propagation. This result is also consistent with previous results from the literature where it was shown that the phase-field fracture approaches are able to recover Griffith's theory when implementing damage boundary conditions on the initial crack (Tanné et al., 2018; Sargado et al., 2018; Molnár et al., 2020; Loiseau and Lazarus, 2025).

The results presented in this section challenge the notion that the phase-field model fully reproduces Griffith's original theory even if ℓ_c tends to zero. Specifically, Griffith compared two states in which the stress field – and consequently the local energy – was singular. In contrast, within the phase-field framework, neither the stress nor the energy density becomes infinite. Thus, even though Griffith's prediction can be recovered when propagating an initially developed process zone, this occurs through the comparison of two regularized (finite) stress states. The model never reverts to a singular stress field, even as $\ell_c \to 0$. At the crack tip, the damage variable always reaches 1, and the corresponding tensile stress vanishes. This constitutes a fundamental difference between the two theories and results in a discrepancy in the predicted critical load, approximately 25% for $\xi_c = 1.5$. This discrepancy decreases as ξ_c decreases, as previously shown in Doitrand and Molnár (2025). Nevertheless, this conundrum raises a deeper question: do truly singular cracks exist, or is there always a local structural rearrangement that introduces a finite process zone? Such a perspective could potentially and partly explain the long-standing difference between the free surface energy (used in surface science) and the fracture surface energy (used in structural mechanics), which describe the same phenomenon but yield significantly different values (Bikerman, 1965; Molnár and Barthel, 2025).

5. Crack initiation through a process zone at a V-notch

The proposed approach is now applied to analyze crack initiation at a V-notch in the presence of an initial process zone. We first examine the initiation of a sharp crack from an existing process zone in Section 5.1, and then focus on regularized crack initiation in Section 5.2.

5.1. Sharp crack initiation

We first evaluate the influence of the process zone on the dimensionless IERR corresponding to sharp crack initiation (Fig. 1(c)). Fig. 4 depicts the decrease in A_{eff} caused by the presence of an initial process zone compared to the case without a process zone. All results are normalized with respect to the configuration where no regularization is applied, denoted by $A_{\text{eff}}(0)$.

Contrary to the opening stress variation at the sharp crack tip before initiation (Fig. 2), the presence of an initial process zone results in a decrease in the dimensionless IERR when increasing any of the three parameters describing the process zone. Indeed, the process zone development before initiation dissipates part of the available elastic strain energy, which tends to decrease the dimensionless IERR and thus to increase the prescribed loading at crack initiation. From Eq. (10), the ratio of the apparent initiation GSIF with and without an initial process zone is computed as $K_{Iapp}(\xi_c)/K_{Iapp}(0) = \left(\frac{A_{\text{eff}}(0)}{A_{\text{eff}}(\xi_c)}\right)^{1-\lambda}\left(\frac{1}{s_\xi}\right)^{2\lambda-1}$. Combining the results shown in Figs. 2 and 4, the variation of the relative increase in apparent initiation GSIF due to the presence of the initial process zone is shown in Fig. 5.

For a given process zone description, the dimensionless stress at the crack tip before initiation is larger than 1 (Fig. 2), which would thus tend to decrease the initiation GSIF compared to the case without process zone. However, this term is counter-balanced by the dimensionless IERR decrease due to the process zone (Fig. 4) so that, overall, the initiation GSIF increases with increasing d_{BC}, ξ_{BC} or ξ.

The proposed approach is now applied to estimate the influence of the initial process zone on the initiation GSIF for several V-notch angles. In the first example (Fig. 6(a) to (c)), the material properties are representative of graphite: $E = 9600$ MPa, $\nu = 0.3$, $\sigma_c = 25$ MPa and $\mathcal{G}_c = 0.14$ MPa.mm (Leguillon and Yosibash, 2017; Ayatollahi and Torabi, 2010). Graphite fracture behavior is quasi-brittle, with the development of a process zone including microcracks (Mostafavi et al., 2013) inducing a non-linearity in the

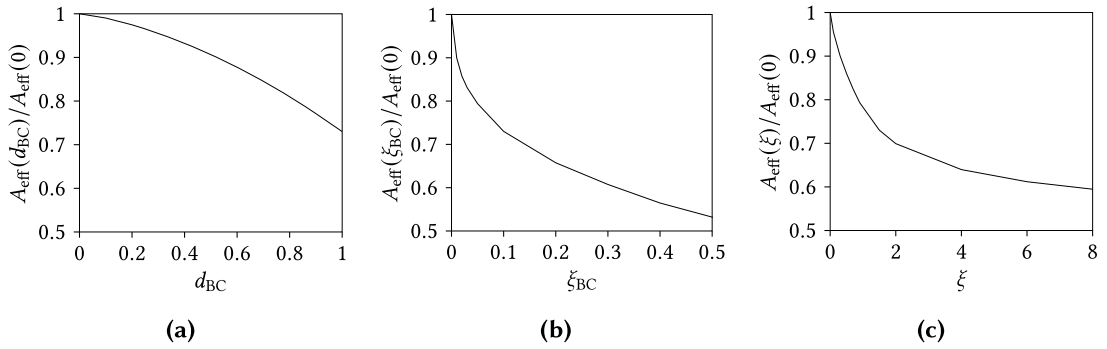

Fig. 4. Variation of the ratio between the dimensionless IERR with (A_{eff}) or without ($A_{\text{eff}}(0)$) an initial process zone (sharp crack initiation at a $\beta = 90$ deg. V-notch) as a function of (a) the Dirichlet phase-field boundary condition magnitude d_{BC} for fixed $\xi_{\text{BC}} = 0.1$ and $\xi = 1.5$, (b) the length over which the boundary conditions are prescribed ξ_{BC}, for fixed $d_{\text{BC}} = 1$ and $\xi = 1.5$ and (c) the regularization length ξ for fixed $\xi_{\text{BC}} = 0.1$ and $d_{\text{BC}} = 1$.

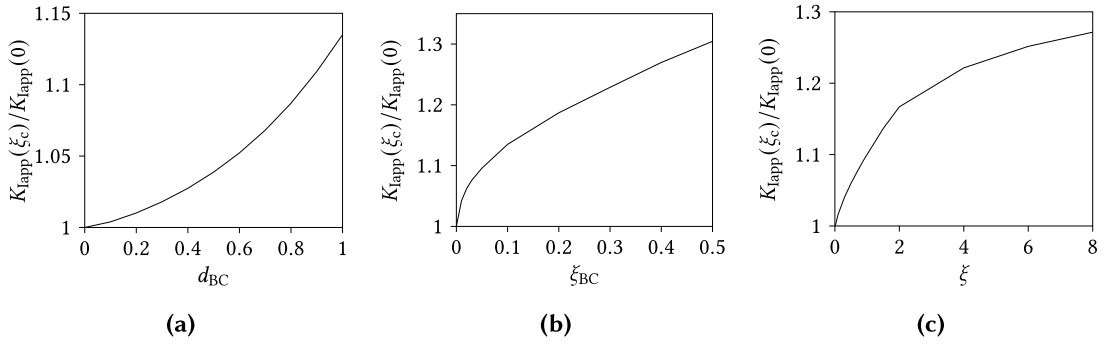

Fig. 5. Variation of the ratio between the apparent initiation GSIF with ($K_{\text{Iapp}}(\xi_c)$) or without ($K_{\text{Iapp}}(0)$) initial process zone (sharp crack initiation at a $\beta = 90$ deg. V-notch) as a function of (a) the Dirichlet boundary condition magnitude d_{BC} for fixed $\xi_{\text{BC}} = 0.1$ and $\xi = 1.5$, (b) the length over which the boundary conditions are prescribed ξ_{BC}, for fixed $d_{\text{BC}} = 1$ and $\xi = 1.5$ and (c) the regularization length ξ for fixed $\xi_{\text{BC}} = 0.1$ and $d_{\text{BC}} = 1$.

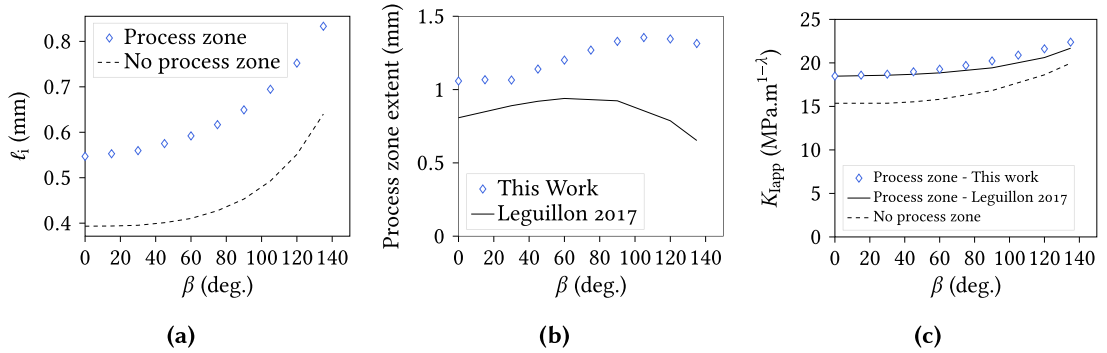

Fig. 6. (a) Variation of the initiation crack length as a function of the V-notch angle with (diamond markers) or without (dashed line) an initial process zone. Comparison of (b) the process zone extent and (c) the apparent GSIF at initiation obtained for different V-notch angles by Leguillon and Yosibash (2017) (continuous line) and in this work (diamond markers).

load-displacement curve prior to crack initiation (Liu et al., 2017; Chen et al., 2017). The initial process zone is described by setting $d_{\text{BC}} = 1$ and $\xi_{\text{BC}} = 0.1$, which provides a similar initiation GSIF value for an initial crack ($\beta = 0$ deg.) to that obtained in Leguillon and Yosibash (2017). The apparent GSIF at crack initiation in the presence of the initial process zone is computed and compared to i) the case without an initial process zone and ii) results obtained by Leguillon and Yosibash (2017) where the process zone was described by a local decrease of the Young's modulus in a circular area surrounding the V-notch.

Regardless of the V-notch angle, the presence of the initial process zone induces an increase in the initiation crack length (Fig. 6(a)) compared to the sharp crack initiation without process zone. The order of magnitude of the initiation crack length is similar to that obtained by Leguillon and Yosibash (2017) who computed initiation crack lengths between approximately 0.8 to 0.9 mm. Nevertheless, a non-monotonic variation of the initiation crack length as a function of the V-notch angle was obtained by Leguillon and Yosibash

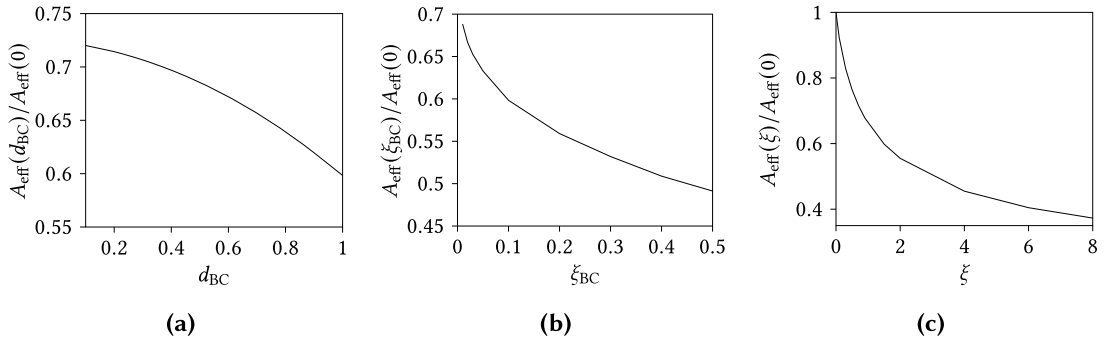

Fig. 7. Variation of the ratio between the dimensionless IERR with or without an initial process zone (regularized crack initiation at a $\beta = 90$ deg. V-notch) as a function of (a) the Dirichlet boundary condition magnitude d_{BC} for fixed $\xi_{\text{BC}} = 0.1$ and $\xi = 1.5$, (b) the length over which the boundary conditions are prescribed ξ_{BC}, for fixed $d_{\text{BC}} = 1$ and $\xi = 1.5$ and (c) the regularization length ξ for fixed $\xi_{\text{BC}} = 0.1$ and $d_{\text{BC}} = 1$.

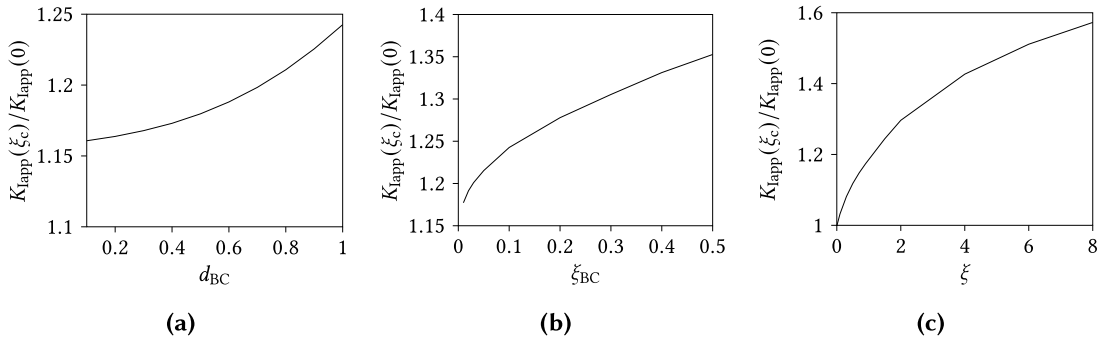

Fig. 8. Variation of the ratio between the apparent initiation GSIF with ($K_{\text{Iapp}}(\xi_{\text{c}})$) or without ($K_{\text{Iapp}}(0)$) initial process zone (regularized crack initiation at a $\beta = 90$ deg. V-notch) as a function of (a) the Dirichlet boundary condition magnitude d_{BC} for fixed $\xi_{\text{BC}} = 0.1$ and $\xi = 1.5$, (b) the length over which the boundary conditions are prescribed ξ_{BC}, for fixed $d_{\text{BC}} = 1$ and $\xi = 1.5$ and (c) the regularization length ξ for fixed $\xi_{\text{BC}} = 0.1$ and $d_{\text{BC}} = 1$.

(2017). Fig. 6(b) shows the variation of the process zone extent along the V-notch bisector as a function of the V-notch angle. The choice of the process zone description results in approximately 1 to 1.3 mm process zone extent along the V-notch bisector, which corresponds to $\xi_{\text{c}} \approx 1.5$ to 2 normalized regularization length at initiation. The order of magnitude of the process zone extent is also similar to that obtained by Leguillon and Yosibash (2017), even if the process zone description was slightly different from the one proposed in this work. Consequently, GSIF at crack initiation similar to that obtained by Leguillon and Yosibash (2017) are also obtained (Fig. 6(c)), the difference slightly increasing for the largest V-notch angles for which the process zone extent is slightly larger in this work. Regardless of the V-notch angle, the presence of the initial process zone induces an increase in the apparent GSIF at crack initiation (see Fig. 6(c)) compared to sharp crack initiation without an initial process zone.

5.2. Regularized crack initiation

We finally study the initiation of a regularized crack in the presence of an initial process zone (Fig. 1(c)). Fig. 7 shows how the process zone influences the dimensionless IERR compared to the case without an initial process zone, as a function of the three parameters describing the process zone. Similarly to sharp crack initiation (Section 5.1), the initial process zone tends to decrease the dimensionless IERR because the available elastic strain energy is partly used for the process zone establishment before regularized crack initiation. As a consequence, the presence of the initial process zone results in an increase in the initiation GSIF, as shown in Fig. 8. When decreasing the regularization length (Fig. 8(c)), the initiation GSIF tends toward that obtained for sharp crack initiation without process zone. When reducing the magnitude of the Dirichlet boundary (Fig. 8(a)) or the length over which the Dirichlet boundary conditions are prescribed (Fig. 8(b)) for fixed regularization length and process zone length, the initiation GSIF tends towards that obtained for regularized crack initiation without the initial process zone (Doitrand and Molnár, 2025).

The proposed approach is finally applied to study regularized crack initiation through an initial process zone and compared to a phase-field calculation, based on the benchmark example of crack initiation under three-point bending in a 90 deg. V-notch specimen (Abaza et al., 2022). The material properties are: 214 GPa Young's modulus, 0.31 Poisson's ratio, 110 J/m^2 critical energy release rate and 583 MPa tensile strength. Results are also compared to the application of the CC to regularized crack initiation without an initial process zone. It was previously shown in Doitrand and Molnár (2025) that in the phase-field calculation, the damage variable attained a $d = 0.4$ maximum value in the process zone just before the sudden force drop corresponding to crack initiation. We thus

Table 1
Normalized regularization length, crack length and apparent GSIF at initiation obtained using the regularized CC considering an initial process zone described by $\xi_{BC} = 0.1$ and $d_{BC} = 0,\ 0.4$ or 1. The apparent GSIF at initiation is also provided for a phase-field (PF) calculation (Doitrand and Molnár, 2025).

	ξ_c	ℓ_i (μm)	K_{Iapp} (MPa.mm$^{0.456}$)	Difference with PF (%)
Phase-Field calculation	–	–	96	–
Regularized CC - $d_{BC} = 0$	1.77	22.3	95.2	0.8
Regularized CC - $d_{BC} = 0.4$	1.51	26.2	96.4	0.4
Regularized CC - $d_{BC} = 1$	1.09	36.5	98.8	2.9

implement the CC using $d_{BC} = 0.4$ and $\xi_{BC} = 0.01$ to be consistent with phase-field observations that show a sharp decrease of the damage variable from 0.4 at the notch tip, and also provide the results for $d_{BC} = 1$ and $d_{BC} = 0$ (no initial process zone) for the sake of comparison. Table 1 shows the results obtained with the different methods.

When increasing d_{BC}, the normalized regularization length tends to decrease whereas the initiation crack length increases, resulting in increasing K_{Iapp} with increasing d_{BC}. Using a $d_{BC} = 1$ Dirichlet boundary condition value yields to a slight overestimate of the initiation GSIF compared to that obtained with the phase-field calculation. A better correspondence is obtained for the regularized CC description including the initial process zone with $d_{BC} = 0.4$, consistently with the process zone observation before initiation in the phase-field calculation shown in Doitrand and Molnár (2025).

6. Conclusion

Crack initiation through a process zone is studied using the CC by combining matched asymptotic expansions and the phase-field regularization. The initial process zone is introduced by prescribing phase-field Dirichlet boundary conditions around the crack initiation location. The process zone description can be adapted by varying the length over which the Dirichlet boundary conditions are imposed, the magnitude of the damage variable and the regularization length. The proposed approach thus offers the possibility of studying sharp or regularized crack initiation in the presence of an initial process zone. Overall, the initial process zone tends to i) mitigate the singular stress field and ii) decrease the incremental energy release rate since part of the stored elastic energy is used for the process zone development. As a consequence, the sharp or regularized crack initiates at a higher apparent GSIF than the one obtained without an initial process zone. The presence of the process zone introduces a stiffness gradient at the V-notch tip. This results in a non-singular stress field for vanishing stiffness at the V-notch tip, or a mitgated singularity for non-vanishing stiffness. This finding thus offers a potential design approach to strengthening materials with geometric singularities against cracking by locally grading their stiffness, even keeping a finite stiffness at the V-notch tip.

Implementing the proposed approach to study the propagation of a regularized semi-infinite crack in infinite medium shows that Griffith's criterion is retrieved provided that Dirichlet boundary conditions are prescribed on the initial sharp crack lips on a zone spanning over at least the regularization length. Otherwise, crack propagation occurs at a higher stress intensity factor. Even though Griffith's prediction can be recovered when propagating a sufficiently large initial process zone, this occurs through the comparison of two regularized stress states. Even when the regularization length tends to zero, the model never reverts to a singular stress field. It thus raises the question about the existence of truly singular cracks, or whether a finite process zone is always present, which would partly explain the long-standing difference between the free surface energy and the fracture surface energy (Bikerman, 1965; Molnár and Barthel, 2025).

In the case of sharp crack initiation at a V-notch, the present results are consistent with those obtained by Leguillon and Yosibash (2017) who introduced an initial process zone by explicitly describing the Young's modulus decrease in a circular zone surrounding the V-notch. In the present work, the process zone description at crack initiation was a priori chosen. Future work will cover the determination of the initial process zone development, which may be studied experimentally based on full-field measurements (Leguillon, 2011) and numerically based on matched asymptotic expansions (Leguillon and Yosibash, 2017). Finally, the regularization length describing the process zone was set based on the material fracture surface according to the previously determined relation (Molnár et al., 2020, 2022). Another perspective of this work is to consider the process zone description independently of the material fracture properties, which will thus result in a 3-parameter criterion to describe quasi-brittle crack initiation. The process zone description could be adapted to represent experimental observations or simulations at a lower scale, such as obtained by molecular dynamics simulations (Molnár and Barthel, 2025).

CRediT authorship contribution statement

Aurélien Doitrand: Writing – original draft, Software, Methodology, Investigation, Conceptualization; **Gergely Molnár:** Writing – review & editing, Software, Investigation, Conceptualization.

Data availability

Data will be made available on request.

Declaration of competing interest

The authors declare that they have no known competing financial interests or personal relationships that could have appeared to influence the work reported in this paper.

Appendix A. Matched asymptotic expansions

The CC is implemented based on matched asymptotic expansions, which aims to determine the displacement fields in two configurations that are studied at two separate scales:

- At the specimen scale, the process zone before initiation and the small crack that initiates through it are neglected because they are small with respect to the specmen dimensions.
- Close to the crack initiation location, we can consider crack initiation at a V-notch configuration disregarding the whole specimen geometry.

The displacement fields obtained for both configurations can be matched in an intermediate zone to obtain the full displacement fields accounting for both the whole specimen geometry and the small crack.

A two-scale problem to be solved under plane strain conditions and linear elasticity is considered. The first problem is studied at the specimen scale, which corresponds to a displacement field noted $\boldsymbol{U}^{\ell,\ell_c,\ell_{BC}}$. The superscripts ℓ, ℓ_c and ℓ_{BC} refer to the presence of an initial process zone of length ℓ_{BC} (the analysis is provided for a fixed value of d_{BC}) and a regularized crack described by the regularizaton length ℓ_c around a sharp crack (nominal length ℓ). The displacement field $\boldsymbol{U}^{\ell,\ell_c,\ell_{BC}}$ is the solution of the set of equations

$$\begin{cases} -\nabla\cdot\underline{\sigma}(\boldsymbol{U}^{\ell,\ell_c,\ell_{BC}})=0, \\ \underline{\sigma}(\boldsymbol{U}^{\ell,\ell_c,\ell_{BC}})=\underline{\underline{C}}:\nabla\boldsymbol{U}^{\ell,\ell_c,\ell_{BC}},\ \underline{\underline{C}} \text{ is the stiffness tensor}, \\ \underline{\sigma}(\boldsymbol{U}^{\ell,\ell_c,\ell_{BC}})\cdot\boldsymbol{n}=\boldsymbol{0} \text{ along the free edges, } \boldsymbol{n} \text{ is the normal vector to the free edges.} \end{cases} \tag{A.1}$$

The initial process zone length, the initiation crack length and the regularization length are supposed to be of the same order of magnitude, and small compared to the specimen dimensions. The validity of the matched asymptotic approach relies on this assumption, which can be checked once the CC has been solved. The presence of the process zone and the regularized crack only influence the displacement and stress distributions close to the V-notch tip. Therefore, the actual solution can be approximated by the solution without the initial process zone and the regularized crack. This solution thus only requires to be corrected close to the V-notch tip. The small correction is determined by solving the problem, close to the crack tip, as detailed in the sequel. The small correction decreases to 0 when ℓ and ℓ_{BC} tend to 0, and when moving away from the V-notch tip. The displacement field is written as

$$\boldsymbol{U}^{\ell,\ell_c,\ell_{BC}}(x_1,x_2)=\boldsymbol{U}^0(x_1,x_2)+\text{ small correction}, \tag{A.2}$$

where $\boldsymbol{U}^0(x_1,x_2)$ is the solution of an idealized problem without process zone and crack. This is the outer field, which is valid except near the V-notch tip. Around a V-notch, the asymptotic displacement field for the opening mode is $K_1 r^\lambda \boldsymbol{u}(\theta)+o(r^\lambda)$, where K_1 is the Generalized Stress Intensity Factor (GSIF). The exponent λ and the corresponding mode $\boldsymbol{u}(\theta)$ are the solution of an eigenvalue problem (Leguillon and Sanchez-Palencia, 1987). The displacement field in the V-notch specimen is written as

$$\boldsymbol{U}^0(x_1,x_2)=\boldsymbol{U}^0(0,0)+K_1 r^\lambda \boldsymbol{u}(\theta)+o(r^\lambda). \tag{A.3}$$

The detailed form of the actual solution $\boldsymbol{U}^{\ell,\ell_c,\ell_{BC}}$ is obtained by rescaling the initial domain by $1/\ell$ and defining the new dimensionless space variables as $y_i=x_i/\ell$. The inner domain is then obtained as ℓ tends to 0. It is an unbounded domain (see Fig. 1(d)) in which :

- The dimensionless crack length is 1
- The dimensionless initial process zone length is $\xi_{BC}=\ell_{BC}/\ell$
- The dimensionless regularization length is $\xi=\ell_c/\ell$

The actual displacement field expands as

$$\boldsymbol{U}^{\ell,\ell_c,\ell_{BC}}(x_1,x_2)=\boldsymbol{U}^{\ell,\ell_c,\ell_{BC}}(\ell y_1,\ell y_2)=F_0(\ell)\boldsymbol{V}^0(y_1,y_2,\xi_{BC},\xi)+F_1(\ell)\boldsymbol{V}^1(y_1,y_2,\xi_{BC},\xi), \tag{A.4}$$

with

$$\lim_{\ell\to 0}\frac{F_1(\ell)}{F_0(\ell)}=0. \tag{A.5}$$

The $\boldsymbol{V}^i$ form the inner field and must match the behaviour of the far field at infinity. There is thus an intermediate zone, close to the V-notch tip in the outer expansion and far from it in the inner expansion, where both expansions given in Eqs. (A.3) and (A.4) hold true. The matching of the terms in Eqs. (A.3) and (A.4) yields

$$\begin{cases} F_0(\ell)=1, \\ \boldsymbol{V}^0(y_1,y_2,\xi_{BC},\xi)=\boldsymbol{U}^0(0,0), \\ F_1(\ell)=K_1\ell^\lambda, \\ \boldsymbol{V}^1(y_1,y_2,\xi_{BC},\xi)\approx\gamma^\lambda\boldsymbol{u}(\theta), \end{cases} \tag{A.6}$$

where $\gamma = r/\ell$ is the normalized polar coordinate. The symbol $\approx$ means that $\boldsymbol{V}^1$ behaves like $\gamma^\lambda \boldsymbol{u}(\theta)$ at infinity, it can be written as

$$\boldsymbol{V}^1(y_1, y_2, \xi_{\mathrm{BC}}, \xi) = \gamma^\lambda \boldsymbol{u}(\theta) + \hat{\boldsymbol{V}}^1(y_1, y_2, \xi_{\mathrm{BC}}, \xi). \tag{A.7}$$

It is necessary to prove that $\hat{\boldsymbol{V}}^1(y_1, y_2, \xi_{\mathrm{BC}}, \xi)$ exists and satisfies the equilibrium equations. Combining Eqs. (A.4) and (A.6) into Eq. (A.1), and since the V-notch faces remain stress free in the inner domain, $\hat{\boldsymbol{V}}^1$ is solution to the following problem

$$\begin{cases} -\nabla_y \cdot \underline{\hat{\sigma}} = 0 \text{ where } \nabla_x = \frac{1}{\ell}\nabla_y, \\ \underline{\hat{\sigma}} = \underline{\underline{C}} : \nabla_y \hat{\boldsymbol{V}}^1, \\ \underline{\hat{\sigma}} \cdot \boldsymbol{n} = 0 \text{ along the V} - \text{notch faces}, \\ \underline{\hat{\sigma}} \cdot \boldsymbol{n} = -(\underline{\underline{C}} : \nabla_y \gamma^\lambda \boldsymbol{u}(\theta)) \cdot \boldsymbol{n} \text{ along the crack faces}, \\ \hat{\boldsymbol{V}}^1 \text{ decreases at infinity.} \end{cases} \tag{A.8}$$

There exists a unique solution with finite energy to this system of equations (Leguillon and Sanchez-Palencia, 1987) (extension of Lax-Milgram theorem to unbounded domains), which decreases to 0 at infinity so that the expansion finally writes

$$\boldsymbol{U}^{\ell,\ell_{\mathrm{c}},\ell_{\mathrm{BC}}}(x_1, x_2) = \boldsymbol{U}^{\ell,\ell_{\mathrm{c}},\ell_{\mathrm{BC}}}(\ell y_1, \ell y_2) = \boldsymbol{U}^0(0,0) + K_{\mathrm{I}}\ell^\lambda[\gamma^\lambda \boldsymbol{u}(\theta) + \hat{\boldsymbol{V}}^1(y_1, y_2, \xi_{\mathrm{BC}}, \xi)]. \tag{A.9}$$

The elastic strain energy variation due to regularized crack initiation is thus written as Leguillon and Sanchez-Palencia (1987), Labossiere and Dunn (1999)

$$-\delta W_{\mathrm{el}} = \Psi(\boldsymbol{U}^{\ell,\ell_{\mathrm{c}},\ell_{\mathrm{BC}}}(x_1, x_2), \boldsymbol{U}^{0,0}(x_1, x_2)), \tag{A.10}$$

where

$$\Psi(\boldsymbol{f}, \boldsymbol{g}) = \frac{1}{2}\int_\Gamma [\underline{\sigma}(\boldsymbol{f}) \cdot \boldsymbol{n} \cdot \boldsymbol{g} - \underline{\sigma}(\boldsymbol{g}) \cdot \boldsymbol{n} \cdot \boldsymbol{f}] ds. \tag{A.11}$$

The path independent integral Ψ is defined on Γ, a closed contour surrounding the studied crack initiation location, starting and ending on the V-notch free faces. The inward normal to this contour is noted $\boldsymbol{n}$. The elastic strain energy variation writes

$$-\delta W_{\mathrm{el}} = \frac{K_{\mathrm{I}}^2}{E}\ell^{2\lambda} A(d_{\mathrm{BC}}, \xi_{\mathrm{BC}}, \xi), \tag{A.12}$$

where $A(\xi, \xi_{\mathrm{BC}})$ depends on the V-notch angle, the dimensionless regularization length and the dimensionless process zone length. It also depends on the Poisson's ratio, as already shown in Doitrand and Molnár (2025), which will not be further studied in this paper. The incremental energy release rate (IERR) for a regularized crack in the presence of a process zone is defined as

$$\mathcal{G}_{\mathrm{inc}} = \frac{-\delta W_{\mathrm{el}}}{\delta \ell_{\mathrm{eff}}} = \frac{K_{\mathrm{I}}^2}{E}\ell^{2\lambda}\frac{A(d_{\mathrm{BC}}, \xi_{\mathrm{BC}}, \xi)}{\delta \ell_{\mathrm{eff}}} = \frac{K_{\mathrm{I}}^2}{E}\ell^{2\lambda-1}\frac{A(d_{\mathrm{BC}}, \xi_{\mathrm{BC}}, \xi)}{\delta \xi_{\mathrm{eff}}(\xi_{\mathrm{BC}}, \xi)} = \frac{K_{\mathrm{I}}^2}{E}\ell^{2\lambda-1} A_{\mathrm{eff}}(d_{\mathrm{BC}}, \xi_{\mathrm{BC}}, \xi). \tag{A.13}$$

The dimensionless IERR $A_{\mathrm{eff}} = A(\xi_{\mathrm{BC}}, \xi)/\delta\xi_{\mathrm{eff}}(\xi_{\mathrm{BC}}, \xi)$ can be obtained by computing the elastic strain energy difference between uncracked and regularized cracked states in the inner domain for a given dimensionless regularization length.

References

Abaza, A., Laurencin, J., Nakajo, A., Meille, S., Debayle, J., Leguillon, D., 2022. Prediction of crack nucleation and propagation in porous ceramics using the phase-field approach. Theor. Appl. Fract. Mech. 119, 103349. https://doi.org/10.1016/j.tafmec.2022.103349

Aranda, M.T., Leguillon, D., 2023. Prediction of failure of hybrid composites with ultra-thin carbon/epoxy layers using the coupled criterion. Eng. Fract. Mech. 281, 109053. https://doi.org/10.1016/j.engfracmech.2023.109053

Ayatollahi, M.R., Torabi, A.R., 2010. Tensile fracture in notched polycrystalline graphite specimens. Carbon 48 (8), 2255–2265. https://doi.org/10.1016/j.carbon.2010.02.041

Barenblatt, G.I., 1959. The formation of equilibrium cracks during brittle fracture. general ideas and hypotheses. axially-symmetric cracks. J. Appl. Math. Mech. 23 (3), 622–636. https://doi.org/10.1016/0021-8928(59)90157-1

Benzeggagh, M.L., Kenane, M., 1996. Measurement of mixed-mode delamination fracture toughness of unidirectional glass/epoxy composites with mixed-mode bending apparatus. Compos. Sci. Technol. 56 (4), 439–449. https://doi.org/10.1016/0266-3538(96)00005-X

Bikerman, J., 1965. Surface energy of solids. Phys. Status Solidi 10 (1), 3–26. https://doi.org/10.1002/pssb.19650100102

Bourdin, B., Francfort, G.A., Marigo, J.-J., 2000. Numerical experiments in revisited brittle fracture. J. Mech. Phys. Solids 48 (4), 797–826. https://doi.org/10.1016/S0022-5096(99)00028-9

Brooks, Z., 2013. Fracture Process Zone: Microstructure and Nanomechanics in Quasi-Brittle Materials. Ph.D. thesis. Massachusetts Institute of Technology.

Camanho, P., Dávila, C., 2002. Mixed-Mode Decohesion Finite Elements for the Simulation of Delamination in Composite Materials. Technical Report. NASA/TM-2002-211737.

Cedolin, L., Dei Poli, S., Iori, I., 1983. Experimental determination of the fracture process zone in concrete. Cem. Concr. Res. 13 (4), 557–567.

Chen, H.H.N., Su, R.K.L., Fok, S.L., Zhang, H.G., 2017. Fracture behavior of nuclear graphite under three-point bending tests. Eng. Fract. Mech. 186, 143–157. https://doi.org/10.1016/j.engfracmech.2017.09.030

Chengyong, W., Peide, L., Rongsheng, H., Xiutang, S., 1990. Study of the fracture process zone in rock by laser speckle interferometry. Int. J. Rock Mech. Min. Sci. Geomechan. Abstr. 27 (1), 65–69.

Ciavarella, M., 2024. Cancelling the effect of sharp notches or cracks with graded elastic modulus materials. J. Mech. Phys. Solids 192, 105809. https://doi.org/10.1016/j.jmps.2024.105809

Cortet, P.-P., Santucci, S., Vanel, L., Ciliberto, S., 2005. Slow crack growth in polycarbonate films. Europhys. Lett. 71 (2), 242.

De Lorenzis, L., Maurini, C., 2022. Nucleation under multi-axial loading in variational phase-field models of brittle fracture. Int. J. Fract. 237 (1), 61–81. https://doi.org/10.1007/s10704-021-00555-6

Denarie, E., Saouma, V.E., Iocco, A., Varelas, D., 2001. Concrete fracture process zone characterization with fiber optics. J. Eng. Mech. 127 (5), 494–502.

Doitrand, A., Duminy, T., Girard, H., Chen, X., 2024. A review of the coupled criterion. J. Theor. Comput. Appl. Mech. https://doi.org/10.46298/jtcam.11072
Doitrand, A., Leguillon, D., Molnár, G., Lazarus, V., 2023a. Revisiting facet nucleation under mixed mode I+III loading with t-stress and mode-dependent fracture properties. Int. J. Fract. 242, 85–106. https://doi.org/10.1007/s10704-023-00703-0
Doitrand, A., Martin, E., Leguillon, D., 2020. Numerical implementation of the coupled criterion: matched asymptotic and full finite element approaches. Finite Element Anal. Des. 168, 103344. https://doi.org/10.1016/j.finel.2019.103344
Doitrand, A., Molnár, G., 2025. Understanding regularized crack initiation through the lens of finite fracture mechanics. Int. J. Fract. 249, 12. https://doi.org/10.1007/s10704-024-00837-9
Doitrand, A., Molnár, G., Estevez, R., Gravouil, A., 2023b. Strength-based regularization length in phase field fracture. Theor. Appl. Fract. Mech. 124, 103728. https://doi.org/10.1016/j.tafmec.2022.103728
Du, J.J., Kobayashi, A.S., Hawkins, N.M., 1990. An experimental-numerical analysis of fracture process zone in concrete fracture specimens. Eng. Fract. Mech. 35 (1–3), 15–27.
Dugdale, D., 1960. Yielding of steel sheets containing slits. J. Mech. Phys. Solids 8 (2), 100–104. https://doi.org/10.1016/0022-5096(60)90013-2
Felger, J., Rosendahl, P.L., Leguillon, D., Becker, W., 2019. Predicting crack patterns at bi-material junctions: a coupled stress and energy approach. Int. J. Solids Struct. 164, 191–201. https://doi.org/10.1016/j.ijsolstr.2019.01.015
Francfort, G., Marigo, J., 1998. Revisiting brittle fracture as an energy minimization problem. J. Mech. Phys. Solids 46 (8), 1319–1342. https://doi.org/10.1016/S0022-5096(98)00034-9
García, I., Leguillon, D., 2012. Mixed-mode crack initiation at a v-notch in presence of an adhesive joint. Int. J. Solids Struct. 49 (15), 2138–2149. https://doi.org/10.1016/j.ijsolstr.2012.04.018
Griffith, A., 1921. The phenomena of rupture and flow in solids. Philosophical Trans. R. Soc. London A: Math. Phys. Eng. Sci. 221 (582–593), 163–198.
Griffith, A., 1924. The theory of rupture. In: First Int. Cong. Appl. Mech, pp. 55–63.
Guo, Z.K., Kobayashi, A.S., Hawkins, N.M., 1993. Further studies on fracture process zone for mode I concrete fracture. Eng. Fract. Mech. 46 (6), 1041–1049.
Haidar, K., Pijaudier-Cabot, G., Dubé, J.-F., Loukili, A., 2005. Correlation between the internal length, the fracture process zone and size effect in model materials. Mater. Struct. 38 (2), 201.
Irwin, G.R., 1948. Fracture dynamics. Fracturing of metals ASM Publi., pp. b147–166.
Irwin, G.R., 1958. Fracture. Springer Berlin Heidelberg. https://doi.org/10.1007/978-3-642-45887-3_5
Jiménez-Alfaro, S., García, I., Doitrand, A., 2025. Review of the matched asymptotic approach of the coupled criterion. Comptes Rendus. Mécanique 353, 339–357. https://doi.org/10.5802/crmeca.285
Jiménez-Alfaro, S., Leguillon, D., 2022. Modelling of glass matrix composites by the coupled criterion and the matched asymptotics approach. the role of a single platelet. Theor. Appl. Fract. Mech. 122, 103650. https://doi.org/10.1016/j.tafmec.2022.103650
Klinsmann, M., Rosato, D., Kamlah, M., McMeeking, R.M., 2015. An assessment of the phase field formulation for crack growth. Comput. Methods Appl. Mech. Eng. 294, 313–330. https://doi.org/10.1016/j.cma.2015.06.009
Knauss, W., 1970. An observation of crack propagation in anti-plane shear. Int. J. Fract. Mech. 6 (2), 183–187. https://doi.org/10.1007/BF00189825
Kristensen, P., Niordson, C., Martínez-Pañeda, E., 2021. An assessment of phase field fracture: crack initiation and growth. Philosophical Trans. R. Soc. A: Math. Phys. Eng. Sci. 379 (2203), 20210021. https://doi.org/10.1098/rsta.2021.0021
Kumar, A., Bourdin, B., Francfort, G., Lopez-Pamies, O., 2020. Revisiting nucleation in the phase-field approach to brittle fracture. J. Mech. Phys. Solids 142, 104027. https://doi.org/10.1016/j.jmps.2020.104027
Labossiere, P. E.W., Dunn, M.L., 1999. Stress intensities at interface corners in anisotropic bimaterials. Eng. Fract. Mech. 62 (6), 555–576. https://doi.org/10.1016/S0013-7944(99)00005-3
Labuz, J.F., Shah, S.P., Dowding, C.H., 1983. Post peak tensile load-displacement response and the fracture process zone in rock. In: The 24th US Symposium on Rock Mechanics (USRMS). American Rock Mechanics Association.
Labuz, J.F., Shah, S.P., Dowding, C.H., 1987. The fracture process zone in granite: evidence and effect. In: International Journal of Rock Mechanics and Mining Sciences & Geomechanics Abstracts. Vol. 24, pp. 235–246.
Lazarus, V., Buchholz, F., Fulland, M., Wiebesiek, J., 2008. Comparison of predictions by mode II or mode III criteria on crack front twisting in three or four point bending experiments. Int. J. Fract. 153 (2), 141–151. https://doi.org/10.1007/s10704-008-9307-2
Leguillon, D., 2001. A criterion for crack nucleation at a notch in homogeneous materials. Comptes Rendus de l'Académie des Sci. Ser. IIB - Mech. 329 (2), 97–102. https://doi.org/10.1016/S1620-7742(01)01302-2
Leguillon, D., 2002. Strength or toughness? a criterion for crack onset at a notch. Eur. J. Mech. A. Solids 21(1), 61–72. https://doi.org/10.1016/S0997-7538(01)01184-6
Leguillon, D., 2008. A damage model based on singular elastic fields. Comptes Rendus Mécanique 336 (3), 283–288. https://doi.org/10.1016/j.crme.2007.10.011
Leguillon, D., 2011. Determination of the length of a short crack at a V-notch from a full field measurement. Int. J. Solids Struct. 48 (6), 884–892. https://doi.org/10.1016/j.ijsolstr.2010.11.020
Leguillon, D., Lacroix, C., Martin, E., 2000. Interface debonding ahead of a primary crack. J. Mech. Phys. Solids 48 (10), 2137–2161. https://doi.org/10.1016/S0022-5096(99)00101-5
Leguillon, D., Murer, S., 2012. Fatigue crack nucleation at a stress concentration point. In: CP2012 Conference Proceedings. Vol. 46. https://www.gruppofrattura.it/ocs/index.php/esis/CP2012/paper/viewFile/9235/5996.
Leguillon, D., Quesada, D., Putot, C., Martin, E., 2007. Prediction of crack initiation at blunt notches and cavities – size effects. Eng. Fract. Mech. 74 (15), 2420–2436. https://doi.org/10.1016/j.engfracmech.2006.11.008
Leguillon, D., Sanchez-Palencia, E., 1987. Computation of Singular Solutions in Elliptic Problems and Elasticity. Wiley, USA.
Leguillon, D., Yosibash, Z., 2017. Failure initiation at V-notch tips in quasi-brittle materials. Int. J. Solids Struct. 122–123, 1–13. https://doi.org/10.1016/j.ijsolstr.2017.05.036
Li, J., Leguillon, D., Martin, E., Zhang, X., 2019. Numerical implementation of the coupled criterion for damaged materials. Int. J. Solids Struct. 165, 93–103. https://doi.org/10.1016/j.ijsolstr.2019.01.025
Liu, D., Mingard, K., Lord, O.T., Flewitt, P., 2017. On the damage and fracture of nuclear graphite at multiple length-scales. J. Nucl. Mater. 493, 246–254. https://doi.org/10.1016/j.jnucmat.2017.06.021
Loiseau, F., Lazarus, V., 2025. How to introduce an initial crack in phase field simulations to accurately predict the linear elastic fracture propagation threshold? J. Theor. Comput. Appl. Mech. . https://doi.org/10.46298/jtcam.15198
Mittelman, B., Yosibash, Z., 2014. Asymptotic analysis of the potential energy difference because of a crack at a V-notch edge in a 3d domain. Eng. Fract. Mech. 131, 232–256. https://doi.org/10.1016/j.engfracmech.2014.07.031
Mittelman, B., Yosibash, Z., 2015. Energy release rate cannot predict crack initiation orientation in domains with a sharp V-notch under mode III loading. Eng. Fract. Mech. 141, 230–241. https://doi.org/10.1016/j.engfracmech.2015.05.008
Molnár, G., Barthel, E., 2025. How glass breaks – damage explains the difference between surface and fracture energies in amorphous silica. arXiv:2412.11817. https://arxiv.org/abs/2412.11817.
Molnár, G., Doitrand, A., Estevez, R., Gravouil, A., 2020. Toughness or strength? Regularization in phase-field fracture explained by the coupled criterion. Theor. Appl. Fract. Mech. 109, 102736. https://doi.org/10.1016/j.tafmec.2020.102736
Molnár, G., Doitrand, A., Estevez, R., Gravouil, A., 2025. A review of characteristic lengths in the coupled criterion framework and advanced fracture models. Comptes Rendus. Mécanique 353, 91–111. https://doi.org/10.5802/crmeca.280
Molnár, G., Doitrand, A., Jaccon, A., Prabel, B., Gravouil, A., 2022. Thermodynamically consistent linear-gradient damage model in abaqus. Eng. Fract. Mech. 266, 108390. https://doi.org/10.1016/j.engfracmech.2022.108390

Molnár, G., Doitrand, A., Lazarus, V., 2024. Phase-field simulation and coupled criterion link echelon cracks to internal length in antiplane shear. J. Mech. Phys. Solids, 105675. https://doi.org/10.1016/j.jmps.2024.105675
Mostafavi, M., McDonald, S.A., Mummery, P.M., Marrow, T.J., 2013. Observation and quantification of three-dimensional crack propagation in poly-granular graphite. Eng. Fract. Mech. 110, 410–420. https://doi.org/10.1016/j.engfracmech.2012.11.023
Neimitz, A., Aifantis, E.C., 1987. On the size and shape of the process zone. Eng. Fract. Mech. 26 (4), 491–503.
Orowan, E., 1949. Fracture and strength of solids. Rep. Progress. Phys. 12, 185–232.
Otsuka, K., Date, H., 2000. Fracture process zone in concrete tension specimen. Eng. Fract. Mech. 65 (2-3), 111–131.
Pham, K., Amor, H., Marigo, J., Maurini, C., 2011. Gradient damage models and their use to approximate brittle fracture. Int. J. Damage Mech. 20 (4), 618–652. https://doi.org/10.1177/1056789510386852
Pham, K., Ravi-Chandar, K., 2014. Further examination of the criterion for crack initiation under mixed-mode I + III loading. Int. J. Fract. 189 (2), 121–138. https://doi.org/10.1007/s10704-014-9966-0
Réthoré, J., Estevez, R., 2013. Identification of a cohesive zone model from digital images at the micron-scale. J. Mech. Phys. Solids 61 (6), 1407–1420.
Rountree, C.L., Bonamy, D., Dalmas, D., Prades, S., Kalia, R.K., Guillot, C., Bouchaud, E., 2010. Fracture in glass via molecular dynamics simulations and atomic force microscopy experiments. Phys. Chem. Glasses-Eur. J. Glass Sci. Technol. Part B 51 (2), 127–132.
Sargado, J., Keilegavlen, E., Berre, I., Nordbotten, J., 2018. High-accuracy phase-field models for brittle fracture based on a new family of degradation functions. J. Mech. Phys. Solids 111, 458–489. https://doi.org/10.1016/j.jmps.2017.10.015
Singh, N., Verhoosel, C., De Borst, R., Van Brummelen, E., 2016. A fracture-controlled path-following technique for phase-field modeling of brittle fracture. Finite Elem. Anal. Des. 113, 14–29. https://doi.org/10.1016/j.finel.2015.12.005
Sommer, E., 1969. Formation of fracture 'lances' in glass. Eng. Fract. Mech. 1 (3), 539–546. https://doi.org/10.1016/0013-7944(69)90010-1
Tanné, E., Li, T., Bourdin, B., Marigo, J., Maurini, C., 2018. Crack nucleation in variational phase-field models of brittle fracture. J. Mech. Phys. Solids 110, 80–99. https://doi.org/10.1016/j.jmps.2017.09.006
Vermilye, J.M., Scholz, C.H., 1998. The process zone: a microstructural view of fault growth. J. Geophys. Res. Solid Earth 103 (B6), 12223–12237.
Vicentini, F., Zolesi, C., Carrara, P., Maurini, C., De Lorenzis, L., 2024. On the energy decomposition in variational phase-field models for brittle fracture under multi-axial stress states. Int. J. Fract. . https://doi.org/10.1007/s10704-024-00763-w
Weißgraeber, P., Leguillon, D., Becker, W., 2016. A review of finite fracture mechanics: crack initiation at singular and non-singular stress raisers. Arch. Appl. Mech. 86(1-2), 375–401. https://doi.org/10.1007/s00419-015-1091-7
Yu, C.-T., Kobayashi, A.S., 1994. Fracture process zone associated with mixed mode fracture of sicw/al2o3. J. Non. Cryst. Solids 177, 26–35.
Yu, Y., Zeng, W., Liu, W., Zhang, H., Wang, X., 2019. Crack propagation and fracture process zone (FPZ) of wood in the longitudinal direction determined using digital image correlation (DIC) technique. Remote Sens. 11 (13), 1562.
Zang, A., Wagner, F.C., Stanchits, S., Janssen, C., Dresen, G., 2000. Fracture process zone in granite. J. Geophys. Res. Solid Earth 105 (B10), 23651–23661.
Zietlow, W.K., Labuz, J.F., 1998. Measurement of the intrinsic process zone in rock using acoustic emission. Int. J. Rock Mech. Min. Sci. 35 (3), 291–299.